



Resonant Neutrino Oscillations ¹

Stephen J. Parke

Fermi National Accelerator Laboratory
P.O. Box 500, Batavia, Illinois, 60510

Abstract

Analytic results are derived for the electron neutrino survival probability after passage through a resonant oscillation region. This survival probability together with a sophisticated model of the production distribution of the solar neutrino sources and the solar electron number density are used to study the effects of resonant neutrino oscillation in the solar interior on the current and proposed solar electron neutrino experiments.

¹Invited talk at the topical conference of the 14th SLAC Summer Institute on Particle Physics, August 5-8, 1986.



Recently, Mikheyev and Smirnov¹ have shown that the matter neutrino oscillations of Wolfenstein² can undergo resonant amplification in the solar interior thereby reducing the flux of electron neutrinos emerging from the Sun. This mechanism may be the solution to the solar neutrino puzzle^{3,4}. Subsequently, Bethe⁵ and others⁶ have refined and restated the Mikheyev and Smirnov idea, pointing out that there are three general regions of parameter space in which the solar electron neutrino flux is sufficiently reduced. In this seminar, I review an analytic calculation⁷ for the electron neutrino survival probability after passage through a resonant oscillation region. Then, I outline a calculation⁸ which uses this result, together with a relatively sophisticated solar model for the production distribution of solar neutrino sources and the solar electron number density, to generate contour plots of electron neutrino capture rates in the mass difference squared - vacuum mixing angle plane, for both chlorine (³⁷Cl) experiment and the proposed gallium (⁷¹Ga) detector.

If neutrinos are massive then the flavor and mass eigenstates are not necessarily identical, however a general neutrino state can always be written in the flavor basis⁹,

$$|\nu(t)\rangle = c_e(t) |\nu_e\rangle + c_x(t) |\nu_x\rangle. \quad (1)$$

For an ultra-relativistic plane wave state propagating in the vacuum, the Dirac equation for this state reduces to the following Schrodinger-like equation,

$$i \frac{d}{dt} \begin{pmatrix} c_e \\ c_x \end{pmatrix} = \frac{\Delta_0}{2} \begin{pmatrix} -\cos 2\theta_0 & \sin 2\theta_0 \\ \sin 2\theta_0 & \cos 2\theta_0 \end{pmatrix} \begin{pmatrix} c_e \\ c_x \end{pmatrix}, \quad (2)$$

after an overall change of phase. $\Delta_0 \equiv \delta m^2/2k$, where $\delta m^2 = (m_2^2 - m_1^2)$, the neutrino squared mass difference, and k is the neutrino energy. θ_0 is the vacuum mixing angle. This evolution equation is trivially solved in terms of the mass eigenstates (the eigenvectors of the two by two matrix). Thus, if a neutrino is produced as an electron neutrino, then the probability of detecting an electron neutrino at some later time, t' , is

$$P_{\nu_e}(t') = \frac{1}{2} + \frac{1}{2} \cos^2 2\theta_0 + \frac{1}{2} \sin^2 2\theta_0 \cos\left(\int^{t'} \frac{\delta m^2}{2k} dt\right). \quad (3)$$

The last term describes the phenomena of vacuum neutrino oscillation, where the oscillation length, L_0 , is given by

$$L_0 = \frac{4\pi k}{\delta m^2} \sim 200km \frac{k}{10MeV} \frac{10^{-4}eV^2}{\delta m^2}. \quad (4)$$

The value of the neutrino energy, 10 MeV, is typical of the neutrinos from the Sun and δm^2 of $10^{-4}eV^2$ will be determined by the electron number density at the solar center.

In matter, the Dirac equation is modified by the weak interactions of the neutrino. Coherent forward scattering contributes to the evolution of this plane wave state. The neutral current interactions of the neutrino with the electrons, protons and neutrons in matter make a contribution proportional to the identity matrix, and therefore only change the overall phase of the neutrino state. Whereas the charge current interactions only effect the electron neutrino component because of the absence of the charge partner to the ν_x in matter and the low energy of the neutrinos. For cold matter (temperature $\ll 1MeV$) this contribution is proportional to the number density of electrons, N_e . Again, after factoring out a piece proportional to the identity matrix, the neutrino evolution equation becomes²

$$i \frac{d}{dt} \begin{pmatrix} c_e \\ c_x \end{pmatrix} = \frac{\Delta_N}{2} \begin{pmatrix} -\cos 2\theta_N & \sin 2\theta_N \\ \sin 2\theta_N & \cos 2\theta_N \end{pmatrix} \begin{pmatrix} c_e \\ c_x \end{pmatrix}. \quad (5)$$

With Δ_N and θ_N determined by

$$\begin{aligned} \Delta_N \cos 2\theta_N &= \Delta_0 \cos 2\theta_0 - \sqrt{2}G_F N_e, \\ \Delta_N \sin 2\theta_N &= \Delta_0 \sin 2\theta_0, \end{aligned}$$

where G_F is the Fermi constant. Of course the sign and the coefficient of the N_e term require careful calculation.

At an electron density, N_e , the matter mass eigenstates are

$$\begin{aligned} |\nu_1, N\rangle &= \cos \theta_N |\nu_e\rangle - \sin \theta_N |\nu_x\rangle \\ |\nu_2, N\rangle &= \sin \theta_N |\nu_e\rangle + \cos \theta_N |\nu_x\rangle \end{aligned} \quad (6)$$

with eigenvalues $E_1 = -\Delta_N/2$ and $E_2 = \Delta_N/2$. Resonance occurs when the difference in these eigenvalues is minimum, that is, when

$$N_e^{res} = \delta m^2 \cos 2\theta_0 / 2\sqrt{2}kG_F. \quad (7)$$

In figure (1) the eigenvalues are plotted as functions of the electron number density. At the resonance density the matter mixing angle $\theta_N^{res} = \pi/4$, which corresponds to maximal mixing between the two flavor states. To convert N_e into a mass density one uses

$$m_N N_e^{res} = (\rho Y_e)^{res} \sim 10^2 g \text{ cm}^{-3} \cos 2\theta_0 \frac{10MeV}{k} \frac{\delta m^2}{10^{-4}eV^2}, \quad (8)$$

where m_N is the nucleon mass, ρ the mass density and Y_e is the ratio of electrons to nucleons. Now we can understand why $\delta m^2 = 10^{-4}eV^2$ is interesting because the mass density of the solar core is $\sim 10^2 g \text{ cm}^{-3}$. In Table I the important parameters for this process are given for a variety of values of the electron number density.

Table I
Parameters for Resonant Neutrino Oscillations

N_e	0	N_e^{res}	$2N_e^{res}$	$\rightarrow \infty$
$E_2 - E_1$	$\frac{\delta m^2}{2k}$	$\frac{\delta m^2}{2k} \sin 2\theta_0$	$\frac{\delta m^2}{2k}$	$\rightarrow \infty$
θ_N	θ_0	$\frac{\pi}{4}$	$\frac{\pi}{2} - \theta_0$	$\rightarrow \frac{\pi}{2}$
L_N	$L_0 = \frac{4\pi k}{\delta m^2}$	$L_0 / \sin 2\theta_0$	L_0	$\rightarrow 0$

The idea of resonant neutrino oscillations as a way of reducing the flux of electron neutrinos and thereby solving the solar neutrino puzzle is to produce at least some of the neutrinos above the resonant density,. This means that these neutrinos are produced mainly in the matter mass eigenstate $|\nu_2, N\rangle$. Then, if the electron number density changes sufficiently slowly as neutrino exits the Sun these neutrinos remains in the $|\nu_2, N\rangle$ state which at zero density is mainly the ν_x neutrino flavor state. That is, there is little crossing between the two matter mass eigenstates.

In figures (2a)-(2d), I have solved the neutrino evolution equation, numerically, for an electron neutrino produced at the center of an exponential electron density distribution which approximates the solar electron density profile. The adiabatic crossing cases are figures (2a) and (2b) whereas in figures (2c) and (2d) there is significant crossing between the two adiabatic states. The transition from adiabatic to non-adiabatic passage occurs when the neutrino state does not have time to change its flavor character as the neutrino passes through resonance. At resonance, the neutrino can change its character in a resonant oscillation length, $L_0/\sin 2\theta_0$. Whereas the width of the resonance region is $R_s \tan 2\theta_0$, for a exponential profile of scale height, R_s . These two lengths are of the same order, for a scale height equal to 0.092 times the radius of the sun, when $\theta_0 \approx 0.01$ for a neutrino energy of 10 MeV and a $\delta m^2 = 10^{-4} \text{eV}^2$.

For a slowly varying electron density, the matter mass eigenstates evolve independently in time; that is $e^{-i \int^t E_1 dt} |\nu_1, N(t)\rangle$ and $e^{-i \int^t E_2 dt} |\nu_2, N(t)\rangle$ are the adiabatic states. Therefore, it is convenient to use these states, as the basis states, in the region for which there are no transitions (away from the resonance region). As a neutrino goes through resonance these adiabatic states may be mixed, but on the other side of resonance, the neutrino state can still be written as a linear combination of these states. That is, a basis state produced at time t , going through resonance at time t_r , and detected at time t' is described by

$$e^{-i \int_t^{t'} E_1 dt} |\nu_1, N(t)\rangle \rightarrow a_1 e^{-i \int_{t_r}^{t'} E_1 dt} |\nu_1, N(t')\rangle + a_2 e^{-i \int_{t_r}^{t'} E_2 dt} |\nu_2, N(t')\rangle$$

or

$$e^{-i \int_t^{t'} E_2 dt} |\nu_2, N(t)\rangle \rightarrow -a_2^* e^{-i \int_{t_r}^{t'} E_1 dt} |\nu_1, N(t')\rangle + a_1^* e^{-i \int_{t_r}^{t'} E_2 dt} |\nu_2, N(t')\rangle$$

where a_1 and a_2 are complex numbers such that $|a_1|^2 + |a_2|^2 = 1$. The relationship between the coefficients, for these two basis states, is due to the special nature of the wave equation, eqn(5). The phase factors have been

chosen so that coefficients a_1 and a_2 are characteristics of the transitions at resonance and are not related to the production and detection of the neutrino state.

Hence, the amplitude for producing, at time t , and detecting, at time t' , an electron neutrino after passage through resonance, is

$$A_1(t) e^{-i \int_{t_r}^{t'} E_1 dt} + A_2(t) e^{-i \int_{t_r}^{t'} E_2 dt}$$

where

$$\begin{aligned} A_1(t) &= \cos \theta_0 (a_1 \cos \theta_N e^{+i \int_{t_r}^{t'} E_1 dt} - a_2^* \sin \theta_N e^{+i \int_{t_r}^{t'} E_2 dt}) \\ A_2(t) &= \sin \theta_0 (a_2 \cos \theta_N e^{+i \int_{t_r}^{t'} E_1 dt} + a_1^* \sin \theta_N e^{+i \int_{t_r}^{t'} E_2 dt}). \end{aligned}$$

Thus the probability of detecting this neutrino as an electron neutrino is given by

$$P_{\nu_e}(t, t') = |A_1(t)|^2 + |A_2(t)|^2 + 2|A_1(t)A_2(t)| \cos\left(\int_{t_r}^{t'} \Delta_N dt + \Omega\right)$$

with $\Omega = \arg(A_1^* A_2)$.

The detection averaged electron neutrino survival probability is easily calculated as

$$\begin{aligned} P_{\nu_e}(t) &= \frac{1}{2} + \frac{1}{2}(|a_1|^2 - |a_2|^2) \cos 2\theta_N \cos 2\theta_0 \\ &\quad - |a_1 a_2| \sin 2\theta_N \cos 2\theta_0 \cos\left(\int_{t_r}^t \Delta_N dt + \omega\right) \end{aligned}$$

with $\omega = \arg(a_1 a_2)$. The last term demonstrates that the phase of the neutrino oscillation at the point the neutrino enters resonance can substantially effect this probability, see figure (3). Therefore, we must also average over the production position, to obtain the fully averaged electron neutrino survival probability^{7,10} as

$$\overline{P_{\nu_e}} = \frac{1}{2} + \left(\frac{1}{2} - P_x\right) \cos 2\theta_N \cos 2\theta_0 \quad (9)$$

where $P_x = |a_2|^2$, the probability of transition from $|\nu_2, N\rangle$ to $|\nu_1, N\rangle$ (or vice versa) during resonance crossing. The non-resonance crossing case is trivially obtained by setting $P_x = 0$.

Also, if the electron neutrinos are produced at a density much greater than the resonance density, so that $\cos 2\theta_N \sim -1$, then

$$\overline{P_{\nu_e}} \approx \sin^2 \theta_0 + P_z \cos 2\theta_0. \quad (10)$$

Thus for small θ_0 , in this limit, the survival probability is just equal to the probability of level crossing during resonance passage.

Similar calculations can also be performed for the case of double resonance crossing (neutrinos from the far side of the sun). Here we must average not only over the production and detection positions of the neutrino but also over the separation between resonances. This sensitivity to the separation of the resonances can be understood as the effect of the phase of the oscillation as the neutrino enters the second resonance region. The fully average probability of detecting an electron neutrino is the same as eqn(9) with P_z replaced by $P_{1z}(1 - P_{2z}) + (1 - P_{1z})P_{2z}$ (the classical probability result). Therefore, the generalization to any number of resonance regions, suitable averaged, is obvious.

To calculate the probability, P_z , I make the approximation that the density of electrons varies linearly in the transition region. That is, a Taylor series expansion is made about the resonance position and the second and higher derivative terms are discarded;

$$N(t) \approx N(t_r) + (t - t_r) \left. \frac{dN}{dt} \right|_{t_r}. \quad (11)$$

In this approximation the probability of transition between adiabatic states was calculated by Landau and Zener¹¹. This is achieved by solving the Schrodinger equation, eqn(5), exactly in this limit. Applying their result to the current situation^{7,12} gives

$$P_z = \exp \left[-\frac{\pi \sin^2 2\theta_0}{2 \cos 2\theta_0} \left. \frac{\delta m^2 / 2k}{|\vec{n} \cdot \nabla \ln N_e|_{res}} \right] \right] \quad (12)$$

where the unit vector, \vec{n} , is in the direction of propagation of the neutrino. Eqn(9) and (12) demonstrate that only the electron number density, at production, and the logarithmic derivative of this density, at resonance, determine the electron neutrino survival probability. It should be emphasized

here, that this result assumes that the neutrino state is produced before significant transitions take place and thus eqn(12) is not valid for neutrinos produced in the transition region.

From eqn(12) the size of the transition region can be determined. There are significant transitions ($P_z > 0.01$) if $\theta_0 < \theta_{crit}$ where θ_{crit} satisfies

$$\frac{\sin^2 2\theta_{crit}}{\cos 2\theta_{crit}} = 3 \frac{1}{\Delta_0} \left| \frac{1}{N} \frac{dN}{dt} \right|_{t_r}. \quad (13)$$

Hence, the maximum separation between the eigenstates for which transitions take place is $\Delta_0 \sin 2\theta_{crit}$. Therefore, the transition region is defined by

$$\Delta_N < \Delta_0 \sin 2\theta_{crit}. \quad (14)$$

This can only happen if $\theta_0 < \theta_{crit}$. In this transition region, the maximum variation of the electron number density from the resonant value is $\pm \delta N$, where

$$\frac{\delta N}{N(t_r)} = \sin 2\theta_{crit}.$$

Thus, the size of the transition region is

$$|t - t_r| = \sin 2\theta_{crit} / \left| \frac{1}{N} \frac{dN}{dt} \right|_{t_r}.$$

This is the maximum $|t - t_r|$ for which the linear approximation must be good, so that eqn(12) gives a reasonable estimate of the probability of crossing. For an exponential density profile, the Taylor series expansion is an expansion in $\sin 2\theta_{crit}$, so that for small θ_{crit} this is an excellent approximation.

Before applying these results to the solar model in detail, let us first consider an exponential electron number density profile which is a good approximation for the solar interior except near the center. In figure (4), I have plotted the electron neutrino survival probability contours at the earth in the $\delta m^2 / 2\sqrt{2}kG_F N_c$ versus $\sin^2 2\theta_0 / \cos 2\theta_0$ plane for such an exponential density profile. Here, the Solar central electron number density, N_c , is also the number density at the point where the neutrinos are produced. This plot depends only on the properties of the sun and this dependency is through the combination $R_s N_c$, where R_s is the scale height. For this figure, I have

used an N_e corresponding to a density of 140g cm^{-3} and $Y_e = 0.7$ and a scale height R_e of 0.092 times the radius of the sun.

Above the line $\delta m^2/2\sqrt{2}kG_F N_e = 1/\cos 2\theta_0$ in this plot, the neutrinos never cross the resonance density on their way out of the sun. Here, the probability of detecting an electron neutrino is close to the standard neutrino oscillation result. Below this line, the effects of passing through resonance comes into play. Inside the 0.1 contour "triangle", there is only a small probability of transitions between the adiabatic states as the neutrino passes through resonance. To the right of this contour triangle, the probability of detecting a neutrino grows, not because of transitions, but because both adiabatic states have a substantial mixture of electron neutrino at zero density. To the left and below the 0.1 contour triangle, the probability grows because here there are significant transitions between the adiabatic states as the neutrino crosses resonance.

More precisely, the solar electron neutrino capture rate for a detector characterized by a electron neutrino capture cross section, $\sigma(E)$, and energy threshold E_0 , is

$$\sum_{\text{processes}} \int_{E_0}^{\infty} \frac{d\Phi_\nu}{dE} \sigma(E) dE. \quad (15)$$

The sum is taken over all neutrino sources in the Sun and $d\Phi_\nu/dE$ is the differential electron neutrino flux of a given source at the earth's surface. To include the reduction in the electron neutrino flux from the Sun due to resonant neutrino oscillations, the differential electron neutrino flux for each process was calculated as

$$\frac{d\Phi_\nu}{dE} \propto W(E) \int_{\text{sun}} dV \overline{P_{\nu_e}} \frac{df}{dV} \quad (16)$$

where $W(E)$ is the standard weak interaction energy distribution for the neutrinos of a given process and df/dV is the fraction of the standard solar model flux coming from a given solar volume element for this process. The solar electron number density profile, $\rho Y_e/m_N$, and the values of df/dV for the various processes were taken from Bahcall's solar model¹³, see figure (5). $d\Phi_\nu/dE$ was normalized for each process by demanding that the energy and solar volume integrations of eqn(15) yield the capture rates given in the

Table II⁴, when $\overline{P_{\nu_e}} \equiv 1$. The cross sections used, for both ^{37}Cl and ^{71}Ga detectors, are given in figure (6).

Table II
Neutrino Sources and Capture Rates (SNU)

Process	$E_{\nu}^{max}(\text{MeV})$	^{37}Cl	^{71}Ga
^8B	14.06	4.3	16
^7Be	0.861(90%) +0.383(10%)	1.0	27
p-p	0.420	0	70
pep	1.44	0.23	2.5
^{13}N	1.199	0.08	2.6
^{15}O	1.732	0.26	3.5
Total		5.9	122

In figures (7) and (8), we present electron neutrino capture rate contours (iso-SNU contours) for the ^{37}Cl and ^{71}Ga experiments as a function of δm^2 and $\sin^2 2\theta_0 / \cos 2\theta_0$ for this solar model. The 3σ deviations from the Davis *et al.*³ result of 2.1 SNU are the 2.4 and 1.8 iso-SNU contour lines in figure (8). The generic structure of these total SNU plots is due to the superposition of triangular iso-SNU contours associated with each individual neutrino source contributing to a given total SNU value. These individual contours owe their shape to the appropriate iso-probability contour, figure (4), and their position is determined by the typical energy scale and production electron density of the individual neutrino source. For each neutrino source the resonance mechanism becomes important, provided $\theta_0 > 0.01$, as soon as δm^2 becomes small enough so that the average resonant electron density for that source is less than the solar electron density at the production site. This occurs when δm^2 is approximately equal to 1.5×10^{-4} , 1.2×10^{-5} , and 3.7×10^{-6} eV² for the ^8B , ^7Be and pp neutrinos respectively. Below these values the individual neutrino sources have contours which are diagonals of slope minus one coming from the form of the transition probability between adiabatic states, eqn(12). The intersection of these diagonal lines with the

turning on of resonance for ${}^8\text{B}$, ${}^7\text{Be}$ and pp is responsible for the shoulders at small $\sin^2 2\theta_0 / \cos 2\theta_0$ in the contour plots. The vertical sections of the contours, at large θ_0 , occur because for large θ_0 both adiabatic states have a large component of electron neutrino.

From figure (8), we see that the results of the ${}^{71}\text{Ga}$ experiment can range from 10 to 110 SNU and still be compatible with the ${}^{37}\text{Cl}$ experiment. In general, a given gallium contour crosses the 2.1 ± 0.3 chlorine contour at least twice and therefore the results of the ${}^{71}\text{Ga}$ experiment will leave a two-fold degeneracy in $(\delta m^2, \theta_0)$ -space. If one accepts the theoretical prejudice against large vacuum angles provided by see-saw models¹⁴, this degeneracy is removed. Unfortunately, the degeneracy is continuous for that region of parameter space corresponding to a ${}^{37}\text{Cl}$ rate of 2.1 ± 0.3 SNU and a ${}^{71}\text{Ga}$ rate greater than 100 SNU. In this region *only* the ${}^8\text{B}$ neutrinos are effected by the resonance phenomena. Also, in this region of parameter space the two experiments will not be able to distinguish between a small temperature change at the solar core and the resonant neutrino oscillation mechanism. This is due to the relatively strong temperature dependence of the ${}^8\text{B}$ neutrino flux¹⁵. It is only when the ${}^{71}\text{Ga}$ SNU rate is depleted below that of merely removing the ${}^8\text{B}$ component (*i.e.*, appreciably less than 110 SNU), so that reduction of the less temperature sensitive neutrinos (${}^7\text{Be}$ and pp) becomes necessary, that the resonant oscillation mechanism becomes a likely solution to the solar neutrino problem.

I wish to thank Rocky Kolb and Terry Walker for discussions.

Fermilab is operated by Universities Research Association Inc. under contract with the United States Department of Energy.

References

1. S.P. Mikheyev and A.Yu. Smirnov, *10th International Workshop on Weak Interactions and Neutrinos*, Savonlinna, Finland(1985); *Nuovo Cimento C9*, 17(1986).
2. L. Wolfenstein, *Phys. Rev. D17*, 2369(1978); *Phys. Rev. D20*, 2634(1979).

3. R. Davis, D.S. Harmer, and K.C. Hoffman, *Phys. Rev. Lett.* **20**, 1205(1968).
4. J.N. Bahcall, B.T. Cleveland, R. Davis, and J.K. Rowley, *Astrophys. J.* **292**, L79(1985).
5. H.A. Bethe, *Phys. Rev. Lett.* **56**, 1305(1986).
6. A. Messiah and S.P. Rosen and M. Spiro, *1986 Massive Neutrinos in Astrophysics and in Particle Physics*, Tignes, January 1986; S.P. Rosen and J.M. Gelb, *Phys. Rev.*, **D34**, 969(1986); E.W. Kolb, M.S. Turner, and T.P. Walker, *Phys. Lett.*, **B175**, 478(1986); V. Barger, R.J.N. Phillips, and K. Whisnant, *Phys. Rev.*, **D34**, 980(1986).
7. S.J. Parke, *Phys. Rev. Lett.* **57**, 1275(1986).
8. S.J. Parke and T.P. Walker, *Phys. Rev. Lett.* (to be published).
9. The other flavor eigenstate could ν_μ or ν_τ .
10. A. Messsiah, *1986 Massive Neutrinos in Astrophysics and in Particle Physics*, Tignes, January 1986.
11. L.D. Landau, *Phys. Z. U.S.S.R.* **1**, 426(1932); C. Zener, *Proc. Roy. Soc.* **A137**, 696(1932).
12. W.C. Haxton, *Phys. Rev. Lett.* **57**, 1271(1986).
13. J.N. Bahcall, W.F. Huebner, S.H. Lubow, P.D. Parker, and R.K. Ulrich, *Rev. Mod. Phys.* **54**, 767(1982).
14. T. Yanagida, *Prog. Theor. Phys.* **B135**, 66(1978); M. Gell-Mann, P. Ramond, and R. Slansky, in *Supergravity*, eds. P. van Nieuwenhuizen and D. Freedman, (North Holland)(1979).
15. In the case where a ^{71}Ga rate of $\gtrsim 100$ SNU is measured, a measurement of the ^8B solar neutrino spectrum (see Rosen and Gelb ref. 6) or the flavor independent solar neutrino flux (see S. Weinberg, contribution to this proceedings) would allow us to distinguish between changes in the solar model and resonant neutrino oscillations.

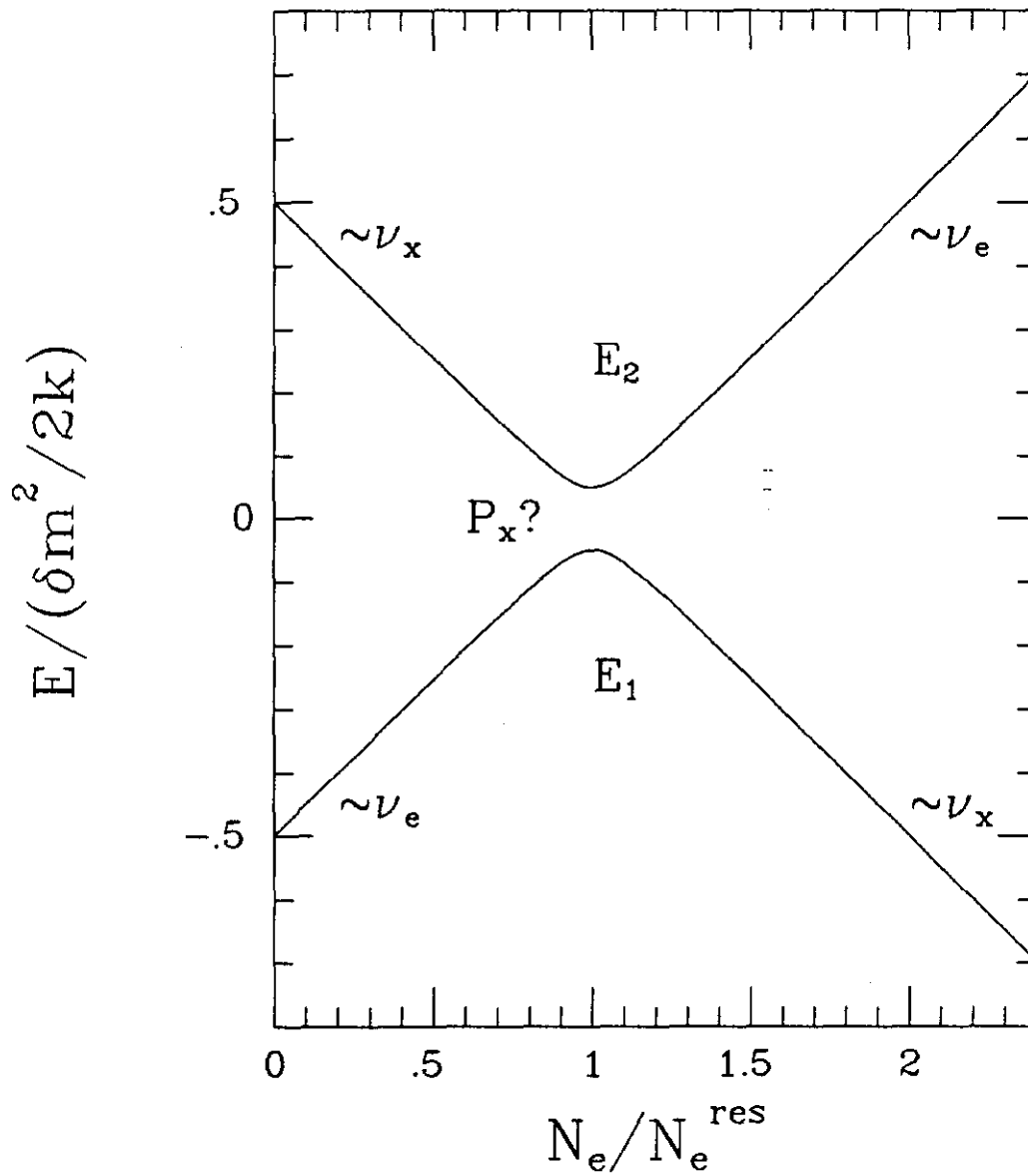


Figure (1): Energy eigenvalues for the matter eigenstates as a function of electron number density.

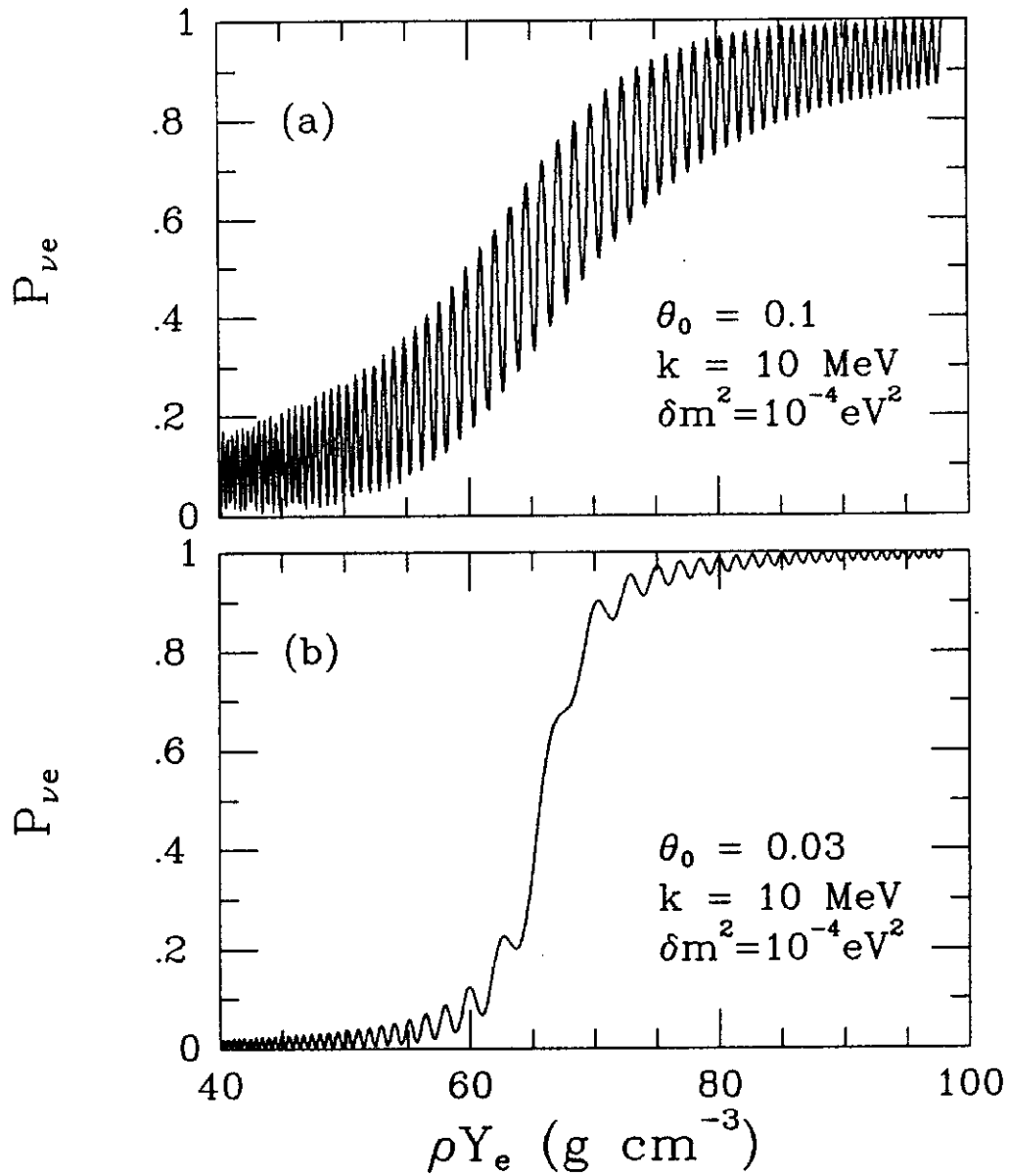


Figure (2a) and (2b): Electron neutrino probabilities as a function of electron density for an electron neutrino produced at the center of the sun. For these values of θ_0 resonance crossing is adiabatic.

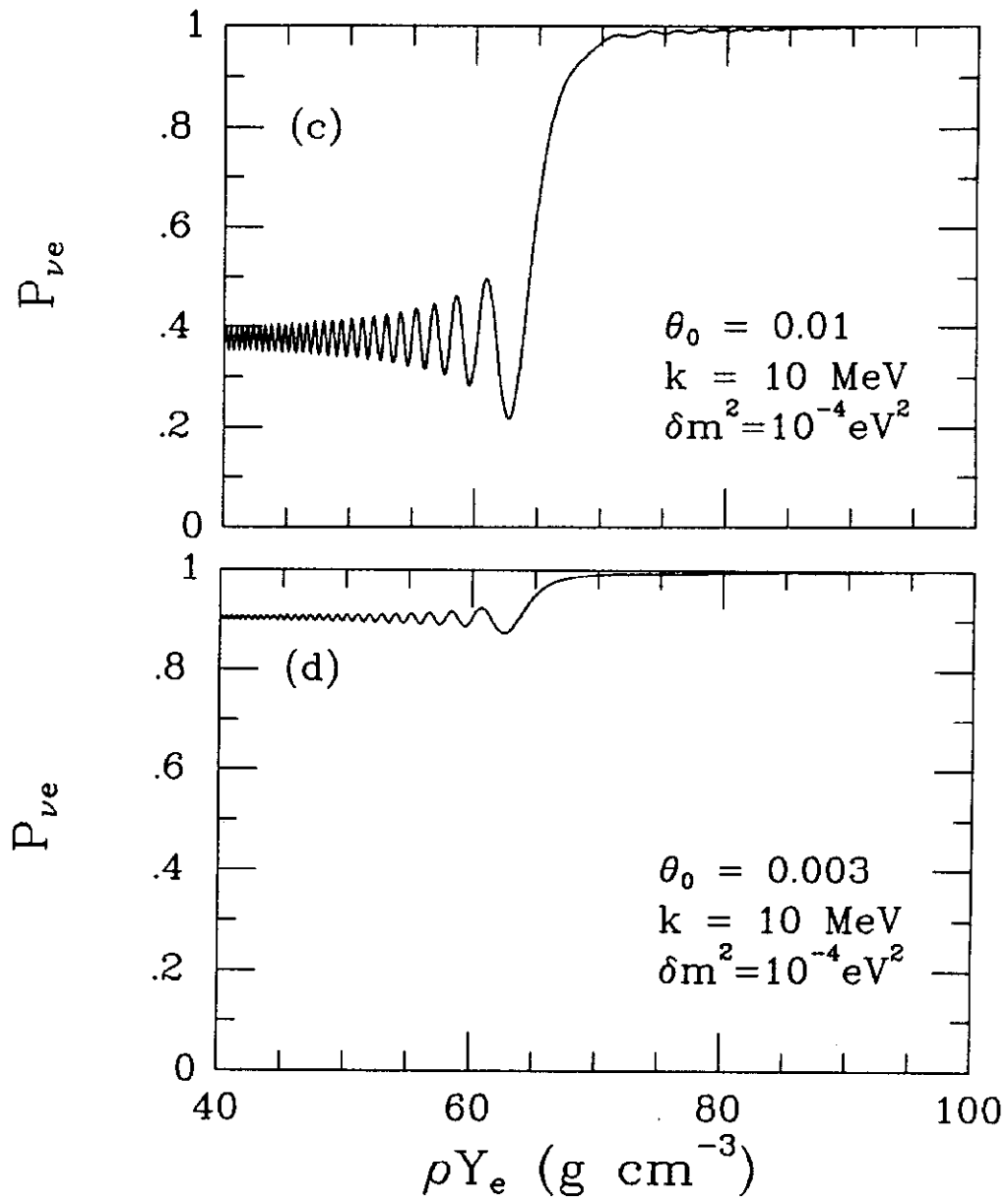


Figure (2c) and (2d): Electron neutrino probabilities as a function of electron density for an electron neutrino produced at the center of the sun. For these values of θ_0 resonance crossing is non-adiabatic.

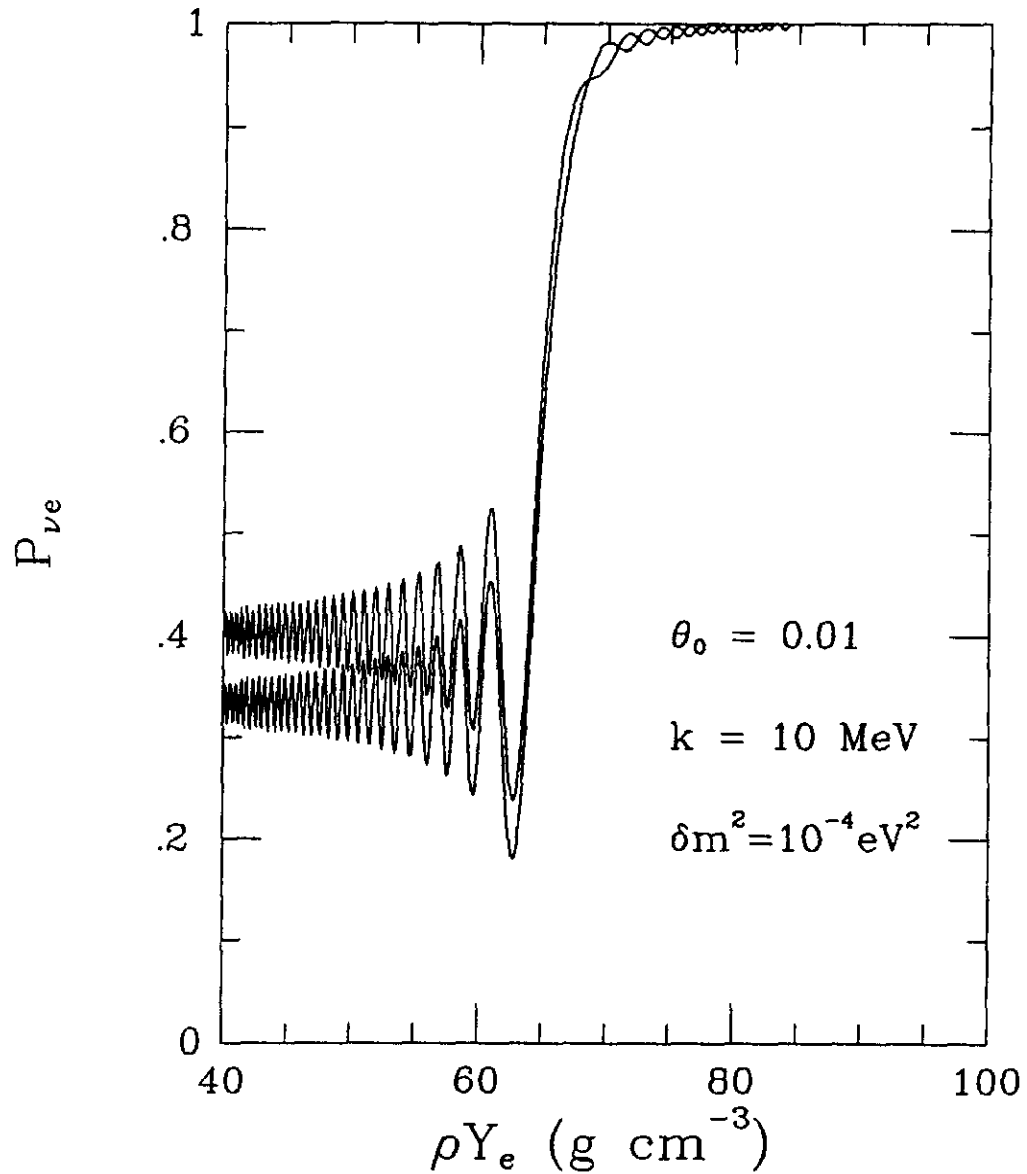


Figure (3): Similar to figure (2) but these two cases were started at $\rho Y_e = 85.0 \pm 0.3 \text{ g cm}^{-3}$. Note the difference in the phase of the oscillation as the neutrino enters the resonance region.

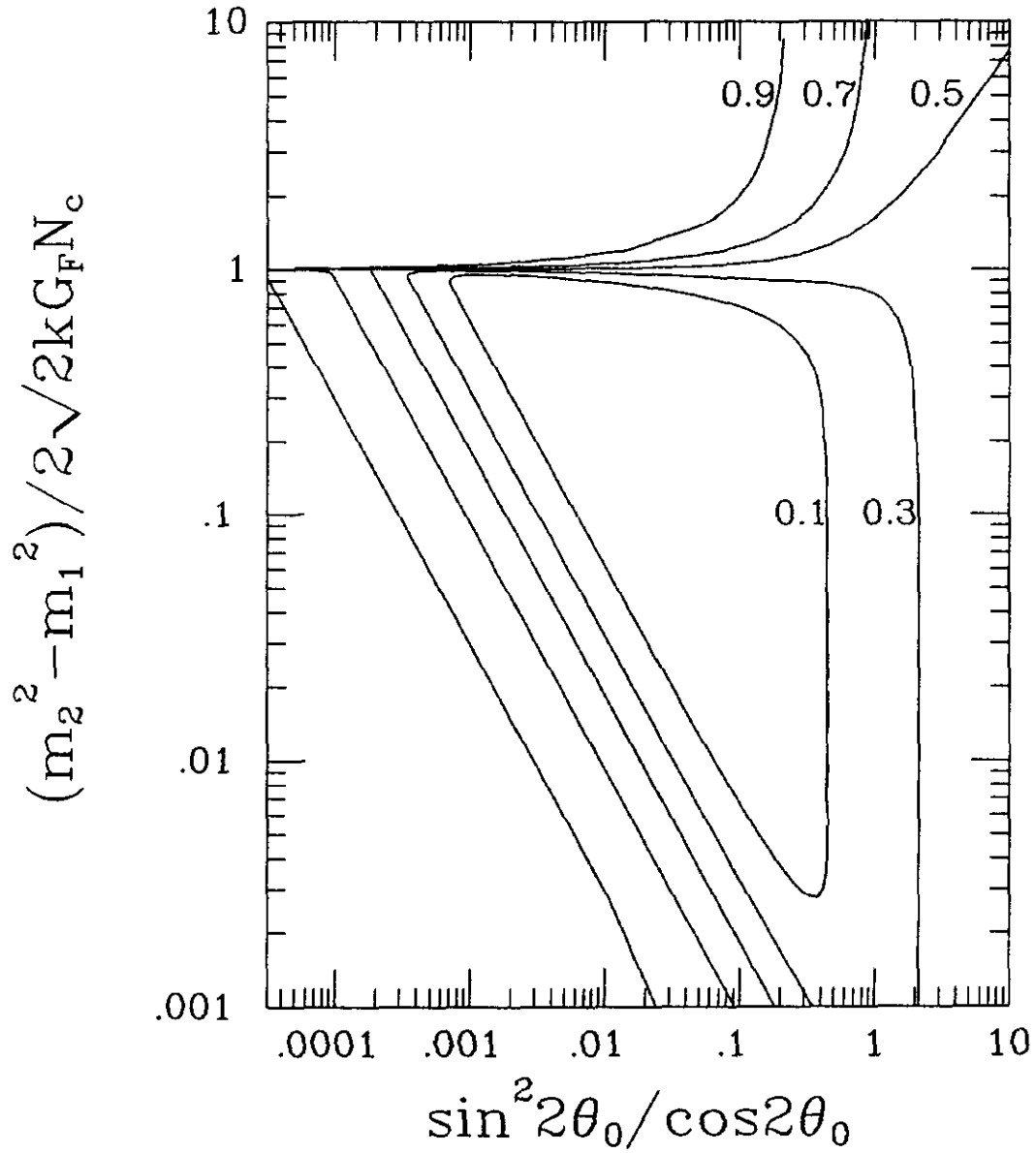


Figure (4): Electron neutrino survival probability contours for an exponential solar electron density profile and an electron neutrino produced at center of the Sun.

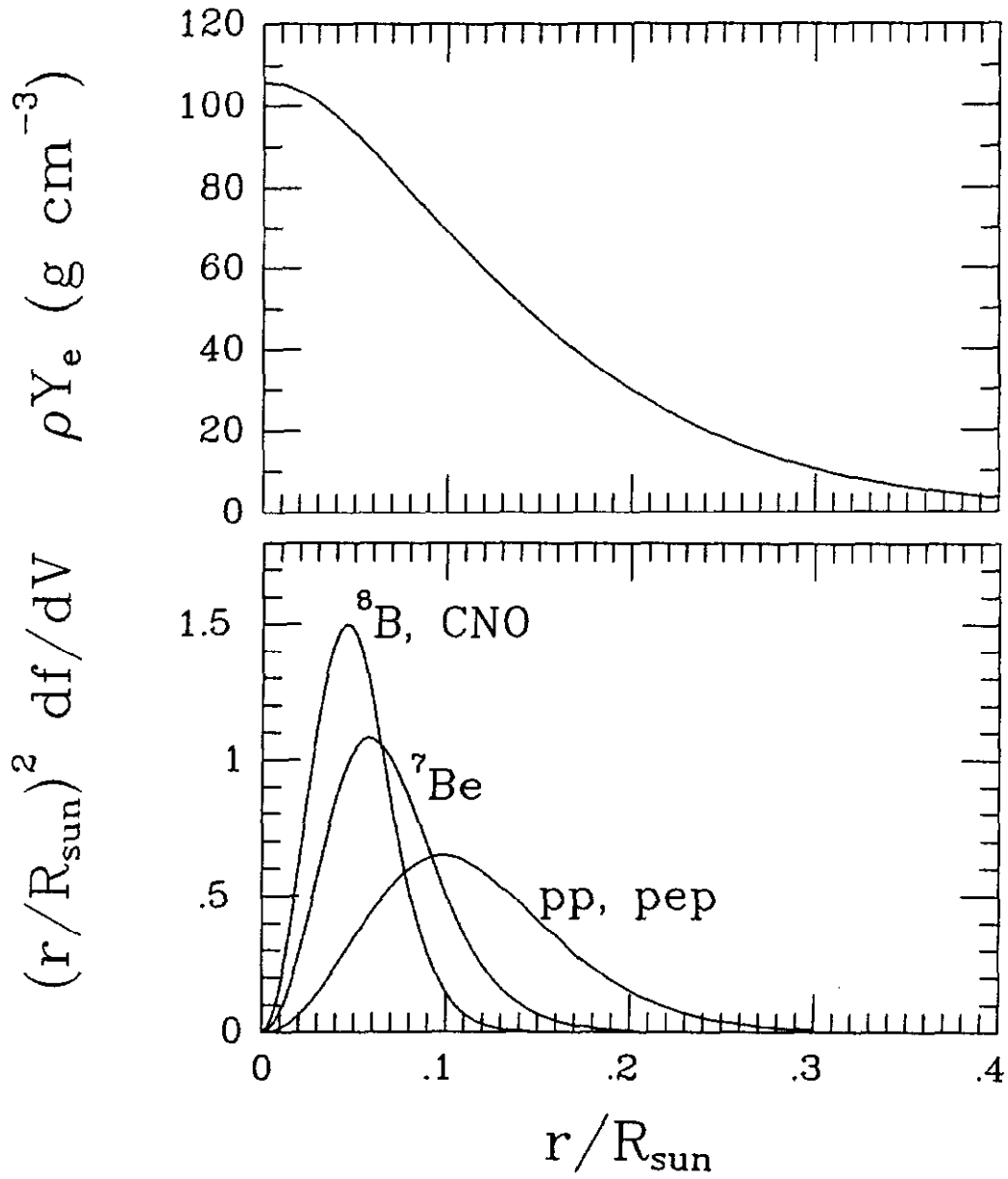


Figure (5): Electron number density and the fractional neutrino emissivity per shell versus the radial distance from the center of the Sun.

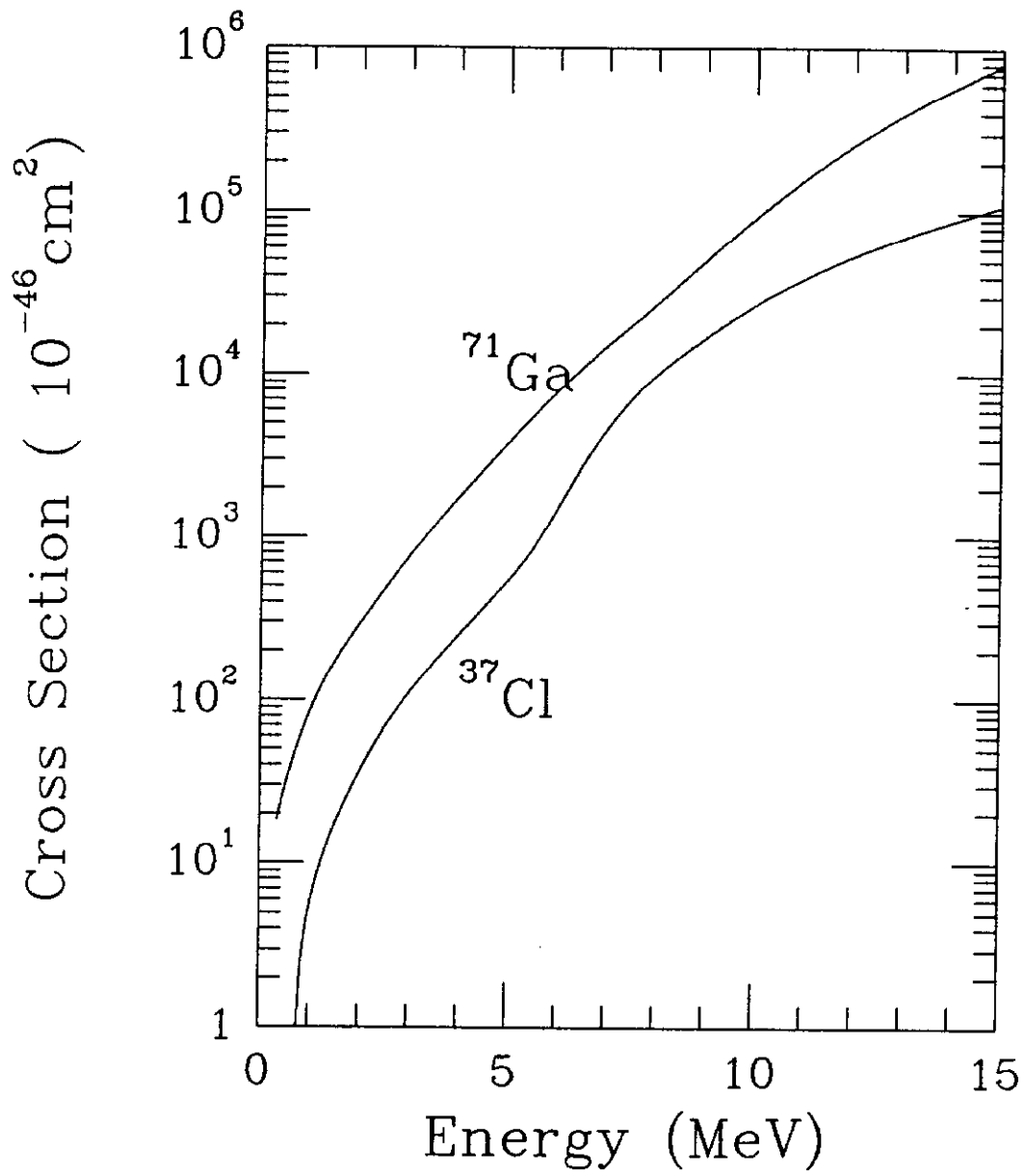


Figure (6): The cross sections for the Chlorine and Gallium detectors as a function of energy.

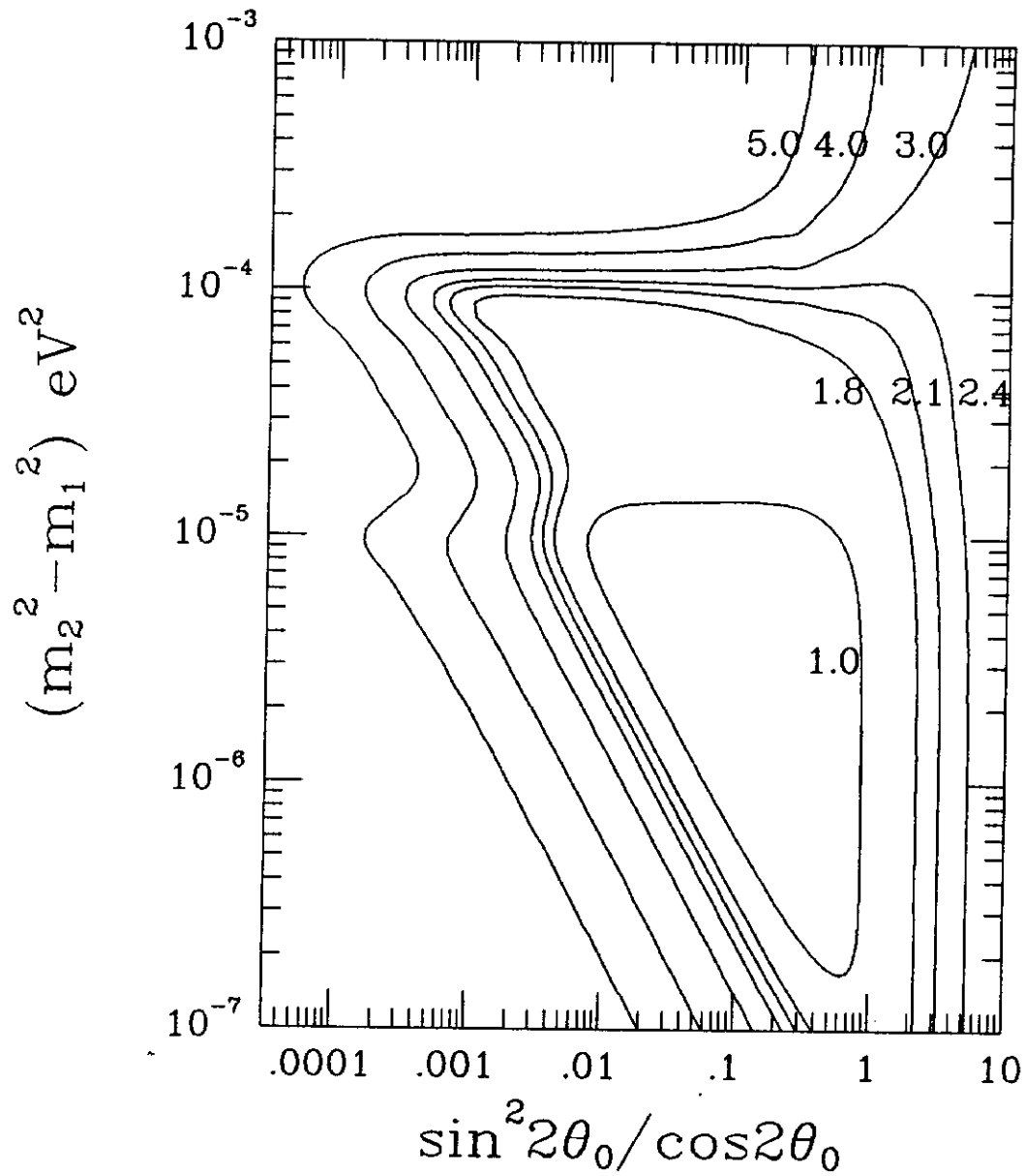


Figure (7): Iso-SNU contours for the ^{37}Cl experiment using Bahcall's solar model. The contours are labeled with their the corresponding SNU values.

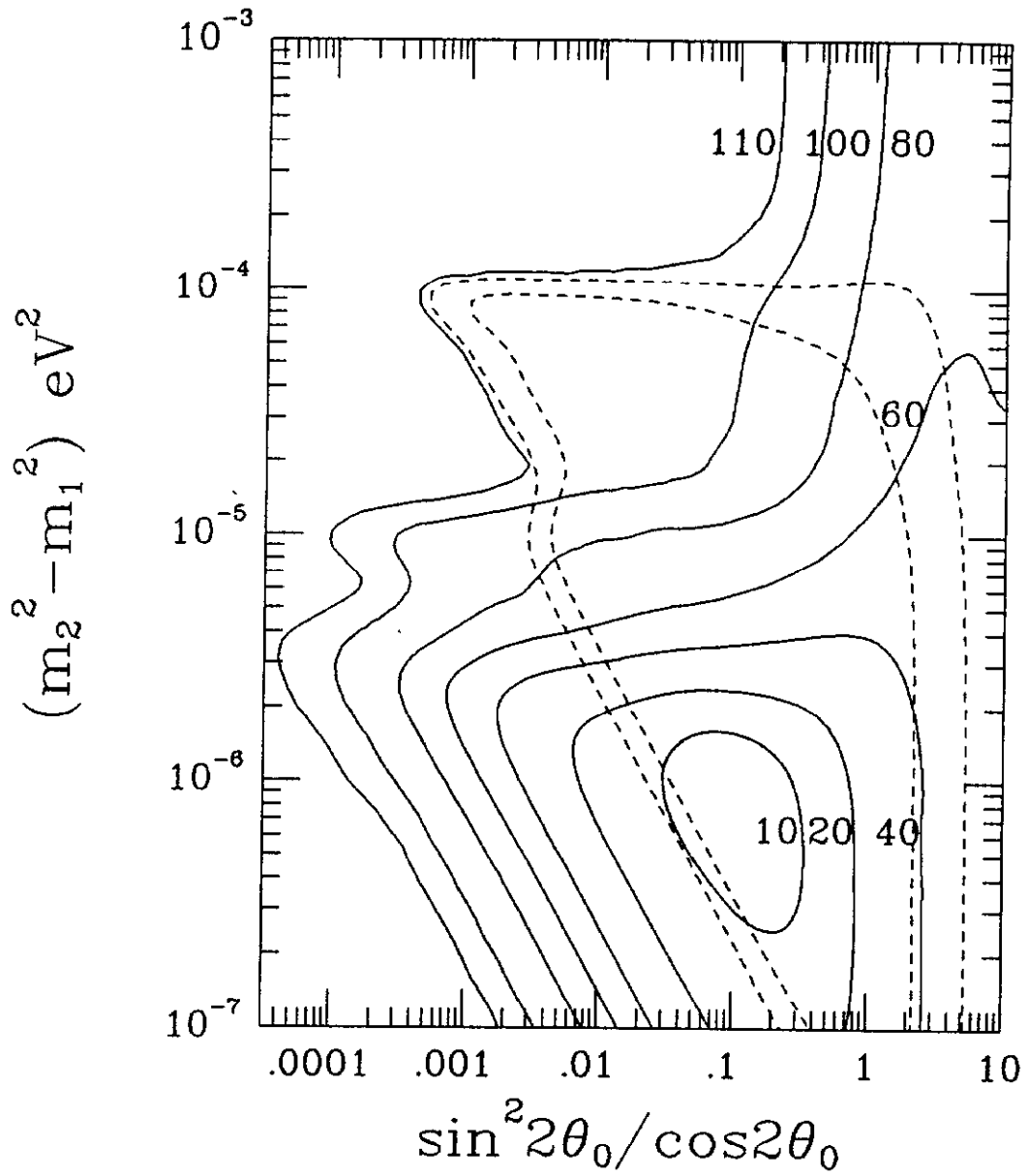


Figure (8): Iso-SNU contours for a ^{71}Ga detector using Bahcall's solar model. The solid contours are labeled with their appropriate ^{71}Ga SNU values and the dashed contours are the 3σ deviations from the Davis ^{37}Cl experimental result.